Journal of Power Sources 258 (2014) 76–82

Contents lists available at ScienceDirect

Journal of Power Sources

journal homepage: www.elsevier.com/locate/jpowsour

$SrMo_{0.9}Co_{0.1}O_{3-\delta}$: A potential anode for intermediate-temperature solid-oxide fuel cells (IT-SOFC)

R. Martínez-Coronado [a,*], J.A. Alonso [b], M.T. Fernández-Díaz [c]

[a] Texas Materials Institute and Materials Science and Engineering Program, The University of Texas at Austin, Austin, TX 78712, United States
[b] Instituto de Ciencia de Materiales de Madrid, C.S.I.C., Cantoblanco, E-28049 Madrid, Spain
[c] Institut Laue Langevin, BP 156X, Grenoble F-38042, France

HIGHLIGHTS

- $SrMo_{0.9}Co_{0.1}O_{3-\delta}$ has been prepared, characterized and tested as anode material.
- Output powers close to 800 mW cm^{-2} at 850 °C with pure H_2 as a fuel.
- "In-situ" neutron powder diffraction at the working conditions of SOFC.
- Metal-like electronic conductivity, as high as 386 S cm^{-1} at $T = 50$ °C.
- Excellent reversibility upon cycling in oxidizing–reducing atmospheres.

ARTICLE INFO

Article history:
Received 25 September 2013
Received in revised form
4 February 2014
Accepted 7 February 2014
Available online 17 February 2014

Keywords:
IT-SOFC
Anode
$SrMoO_3$ perovskite
$SrMoO_4$ scheelite

ABSTRACT

$SrMo_{0.9}Co_{0.1}O_{3-\delta}$ oxide has been prepared, characterized and tested as anode material in single solid-oxide fuel cells (SOFC), yielding output powers close to 800 mW cm^{-2} at 850 °C with pure H_2 as a fuel. This excellent performance is accounted for the results of an "in-situ" neutron powder diffraction (NPD) experiment, at the working conditions of a SOFC, showing the presence of a sufficiently high oxygen deficiency, with large displacement factors for oxygen atoms that suggest a large lability and mobility, combined with a huge metal-like electronic conductivity, as high as 386 S cm^{-1} at $T = 50$ °C. Besides, the oxidation of the perovskite gives rise to a new oxygen deficient scheelite-like phase with formula $SrMo_{0.9}Co_{0.1}O_{4-\delta}$ with Mo(VI), which has been studied by NPD and thermal analysis as far as crystal structure and composition are concerned. An adequate thermal expansion coefficient for both (oxidized and reduced) phases, an excellent reversibility upon cycling in oxidizing–reducing atmospheres and a good chemical compatibility with the electrolyte ($La_{0.8}Sr_{0.2}Ga_{0.83}Mg_{0.17}O_{3-\delta}$; LSGM) make this oxide a good candidate for anode in intermediate-temperature SOFC (IT-SOFCs).

1. Introduction

Solid oxide fuel cells (SOFC) are electrochemical devices with a high energy-conversion efficiency, which makes them quite attractive as a promising technology for electrical energy generation. Additionally, SOFC can utilize a wide variety of fuels (H_2, hydrocarbons, syngas…) which constitutes an added advantage. However, one of the major challenges for the development of SOFCs as economically-viable devices is the decrease in the operating temperature (to the 550–850 °C range) without incurring in the deterioration of the effectiveness of the cell [1,2]. One of the rate-limiting steps of this electrochemical conversion is the fuel-oxidation reaction, which is catalyzed at the anode. For this task, novel mixed ionic-electronic conductor (MIEC) oxides with sufficient stability under the reducing atmosphere of the fuel are being developed to replace the conventional anode materials.

The traditional Ni-cermet (mixture of NiO and electrolyte oxide powders) anodes show excellent electrochemical performance, however these anodes are susceptible to sulfur poisoning and suffer from sintering problems during the cell operation [3–5]; alternative anode materials are attractive to reduce cost and to increase the applicability to other fuel streams, including hydrocarbons. Among various kinds of oxide materials, those with perovskite structure have received great attention for SOFC electrodes due to their excellent electronic properties with considerable ionic conductivity [6–8].

Several works have demonstrated a great performance of Mo-based double perovskites operating in H_2 or CH_4 as a fuel [9–11]. $AMoO_3$ (A = Ca, Sr, Ba) perovskites [12,13], nominally containing

* Corresponding author. Tel.: +1 512 471 1646; fax: +1 512 471 7681.
E-mail address: rmartinez@icmm.csic.es (R. Martínez-Coronado).

http://dx.doi.org/10.1016/j.jpowsour.2014.02.031
0378-7753/

Mo^{4+} cations, have adequate electron transfer energies as to screen and cancel the electrostatic energy accompanied by the electron transfer. The $SrMoO_3$ cubic perovskite (containing Mo(IV) at the B-sites of the ABO_3 perovskite structure) has been reported to present one of the highest electrical conductivity values at room temperature for a ceramic material ($\sim 10^4$ S cm^{-1}) [14]; however this oxygen-stoichiometric oxide cannot exhibit the required oxygen-ion diffusion and conductivity. In previous works we have demonstrated by suitably doping with trivalent elements at the B-site in this material ($SrMo_{1-x}M_xO_{3-\delta}$ (M = Fe, Cr)) [15,16] that it is possible to induce the necessary oxygen vacancies. An adequate mixed ionic-electronic conductivity was achieved giving rise to excellent anodes material in SOFC.

Furthermore, cobalt-based perovskite compounds have attracted a lot of attention as IT-SOFCs electrodes due to their mixed-conducting characteristics and high ion-conductivity in the intermediate temperature range [17,18]; the ability to present mixed oxidation states and the important covalent character of the Co–O bonds are the essential factors. Taking advantage of both Mo and Co-perovskites properties, the aim of this work has been to replace Mo by aliovalent Co ions at the B-position of the $SrMoO_3$ oxide. The purpose has been to induce the formation of anionic vacancies and to improve the oxygen-ion mobility thus promoting oxygen conduction, both essential factors to obtain an excellent electrode in SOFC.

In the present work we show that the $SrMo_{0.9}Co_{0.1}O_{3-\delta}$ oxide can be successfully used as anode in SOFCs with H_2 as a fuel; for this purpose, single cells in an electrolyte-supported configuration have been set up and tested with $SrMo_{0.9}Co_{0.1}O_{3-\delta}$ (SMCO) as anode, $SrCo_{0.8}Fe_{0.2}O_{3-\delta}$ (SCFO) as cathode and $La_{0.8}Sr_{0.2}Ga_{0.83}Mg_{0.17}O_{3-\delta}$ (LSGM) as electrolyte. In order to correlate the crystal structure and the properties of the anode material, a structural characterization has been carried out from NPD data, which is a powerful tool [19] to examine, *in situ*, the specimen under the usual conditions of a SOFC (under low pO_2 atmosphere for the anode and at the working temperature). Therefore, we report on the results of a complete characterization study including the electrical performance of the single cell, dilatometry, conductivity, chemical compatibility, thermal analysis, red-ox reversibility and scanning electron microscopy after the single-cell test.

2. Experimental

$SrMo_{0.9}Co_{0.1}O_{3-\delta}$ polycrystalline powders were prepared by soft-chemistry procedures. Stoichiometric amounts of $Sr(NO_3)_2$, $(NH_4)_6Mo_7O_{24}\cdot 4H_2O$ and $Co(NO_3)_2$ were dissolved in citric acid and some drops of nitric acid. The solution was then slowly evaporated, leading to organic resins that contain a homogeneous distribution of the involved cations. The formed resins were dried at 120 °C and decomposed at 600 °C for 12 h in order to eliminate the organic materials and the nitrates. A final treatment at 1050 °C in a tubular furnace under a H_2(5%)/N_2 flow for 15 h led to the formation of the wanted perovskite oxide. Subsequent treatments at higher temperatures (1100 °C) in 5%H_2 demonstrated that the obtained perovskite is stable and the formation of secondary phases was not observed.

The initial characterization of the product was carried out by XRD with a Bruker-axs D8 Advanced diffractometer (40 kV, 30 mA), controlled by a DIFFRACT^{PLUS} software, in Bragg–Brentano reflection geometry with Cu K_α radiation (λ = 1.5418 Å) and a PSD (Position Sensitive Detector). A filter of nickel allows the complete removal of Cu K_β radiation. The slit system was selected to ensure that the X-ray beam was completely within the sample for all 2θ angles. For the structural refinement, NPD patterns were collected at the D2B diffractometer of the Institut Laue-Langevin, Grenoble, with a wavelength λ = 1.594 Å, at 25, 300, 600 and 850 °C. About 2 g of the sample were contained in a vanadium can and placed in the isothermal zone of a furnace with a vanadium resistor operating under vacuum ($P_{O_2} \approx 10^{-6}$ Torr), and the counting time was 2 h per pattern in the high-intensity mode. The NPD data were analyzed by the Rietveld method [20] with the FULLPROF program [21]. A pseudo-Voigt function was chosen to generate the line shape of the diffraction peaks. The following parameters were refined in the final run: scale factor, background coefficients, zero-point error, pseudo-Voigt corrected for asymmetry parameters, positional coordinates and isotropic thermal factors for all the atoms. The coherent scattering lengths for Sr, Co, Mo, and O were 7.02, 2.49, 6.72, and 5.803 fm, respectively [21].

Thermal analysis was carried out in a Mettler TA3000 system equipped with a TC10 processor unit. Thermogravimetric (TG) curves were obtained in a TG50 unit, working at a heating rate of 10 °C min^{-1}, in an oxygen flow of 0.3 L min^{-1}. The heating rate was 10 °C min^{-1}, using about 50 mg of sample in each experiment.

Measurements of the thermal expansion coefficient and electrical conductivity required the use of sintered samples. The relative density was 90–95%. Thermal expansion of the sintered samples was performed in a dilatometer Linseis L75HX1000, between 300 and 800 °C in H_2(5%)/N_2(95%). The conductivity was measured between 25 and 850 °C in H_2(5%)/N_2(95%), by the four-point method in bar-shaped pellets under DC currents between 0.1 and 0.5 A. The currents were applied and collected with a Potentiostat–Galvanostat AUTOLAB PGSTAT 302 from ECO CHEMIE.

Single-cell tests were carried out using LSGM pellets as electrolyte, $SrCo_{0.8}Fe_{0.2}O_{3-\delta}$ (SCFO) as cathode material, and $SrMo_{0.9}Co_{0.1}O_{3-\delta}$ (SMCO) as anode material. The LSGM pellets of 20-mm diameter were sintered at 1450 °C for 20 h and then polished with a diamond wheel to a thickness of 300 μm. $SrCo_{0.8}Fe_{0.2}O_3$ powders were prepared by soft-chemistry procedures, as the title compound, with stoichiometric amounts of $Sr(NO_3)_2$, $Co(NO_3)_2$ and $C_2FeO_4\cdot 2H_2O$. A final treatment at 1000 °C in air for 12 h led to the formation of the pure perovskite oxide. $La_{0.4}Ce_{0.6}O_{2-\delta}$ (LDC) was used as a buffer layer between the anode and the electrolyte in order to prevent the possible interdiffusion of ionic species. Inks of LDC, SMCO and SCFO were prepared with a binder (V-006 from Heraeus). LDC ink was screen-printed onto one side of the LSGM disk followed by a thermal treatment at 1300 °C in air for 1 h. SMCO was subsequently screen printed onto the LDC layer and fired at 1100 °C in air for 1 h. SCFO was finally screen printed onto the other side of the disk and fired at 1100 °C in air for 1 h. The working electrode area of the cell was 0.24 cm^2 (0.6 × 0.4 cm). Pt or Au gauze with a small amount of Pt or Au paste in separate dots was used as current collector at both the anodic and the cathodic sides for ensuring electrical contact. The cells were tested in a vertical tubular furnace at 750, 800 and 850 °C; the anode side was fed with pure H_2, with a flow of 20 ml min^{-1}, whereas the cathode worked in an air flow of 100 ml min^{-1}. The fuel-cell tests were performed with an AUTOLAB 302N Potentiostat/Galvanostat by changing the voltage of the cell from the OCV ("Open current voltage") to 0.1 V, with steps of 0.010 V, holding 10 s at each step. The current density was calculated by the recorded current flux through the effective area of the cell (0.24 cm^2). Each V–I (voltage–current density) scan corresponds to one cycle.

Scanning electron microscopy (SEM) images were carried out with a Hitachi S-3000N and an analyzer from Oxford Instrument, model INCAx-sight.

3. Results and discussion

3.1. Crystallographic characterization

$SrMo_{0.9}Co_{0.1}O_{3-\delta}$ oxide was obtained as a well-crystallized powder. A single-phase cubic perovskite phase was identified

from laboratory X-ray diffraction (XRD), as shown in Fig. 1; no impurity phases were detected.

A neutron powder diffraction (NPD) study at room temperature (25 °C) and high temperature (up to 850 °C) for $SrMo_{0.9}Co_{0.1}O_{3-\delta}$ was useful to investigate the structural details in relation to the performance of this material as anode in IT-SOFC. The crystal structure, at room temperature, was defined in the *Pm-3m* space group (No. 225), $Z = 1$; Sr atoms are located at *1b* (½,½,½) positions, Mo and Co are distributed at random at *1a* (0,0,0), and oxygen atoms O are located at *3d* (½,0,0). The occupancy factors of oxygen atoms were also refined in the final run exhibiting a negligible oxygen deficiency. Assuming that the Co ions are in a trivalent oxidation state, the absence of oxygen vacancies observed at room temperature indicates that the introduction of Co^{3+} drives to a slight increase of the Mo oxidation state, giving rise to a mixed-valence state Mo(IV)–Mo(V). The refined Mo/Co ratio for this sample leads to the final $SrMo_{0.92(1)}Co_{0.08(1)}O_{3.00(1)}$ stoichiometry, with a $Mo^{+4.09}$ average oxidation state. Fig. 2 illustrates the good agreement between the observed and calculated NPD patterns for (nominal) $SrMo_{0.9}Co_{0.1}O_3$ at room temperature. The inset of Fig. 2 illustrates the cubic perovskite unit cell. Table 1 summarizes the atomic, displacement parameters, discrepancy factors and inter-atomic distances after the Rietveld refinements of the structure at room temperature from NPD data.

The unit-cell parameter obtained for the sample at room temperature is $a = 3.9702(6)$ Å, which is fairly close to the value reported in the literature for $SrMoO_3$, $a = 3.9762(3)$ Å [22]. The introduction of a smaller cation at B-site ($^{VI}Co^{3+}$ (0.615 Å) *vs* $^{VI}Mo^{4+}$ (0.65 Å) [23]) entails the reduction of the unit-cell. As a reference, the aristotype (simple-cubic sub-cell) of the double-perovskite Sr_2MoCoO_6, which crystallizes in the *Fm-3m* (No. 225) space group, has a lattice parameter of 3.9634 Å [24], indicating the tendency of the unit-cell to shrink upon Co-doping at the Mo site. The obtained value for the (Mo,Co)–O1 interatomic distance, which is 1.9856 (3) Å (Table 1), is slightly smaller than that expected from the ionic radii of Co^{3+} (0.615 Å), Mo^{4+} (0.65 Å) and O^{-2} (1.40 Å) [23], of 2.047 Å for the determined crystallographic formula, which agrees with the proposed hole-doping effect on Mo ions (average valence +4.09). As expected, the <Mo,Co–O> bond length is smaller than that of the parent $SrMoO_3$ perovskite [22], of 1.9881(1) Å, also supporting the mentioned hole-doping effect.

Finally, the thermal evolution of the crystal structure under the anode conditions in a SOFC was evaluated by NPD for $SrMo_{0.9}Co_{0.1}O_{3-\delta}$. For this purpose, the sample was contained in a vanadium can under high vacuum (10^{-6} Torr) and NPD data were collected *in situ* in a furnace at 300, 600 and 850 °C. The NPD patterns, illustrated in Fig. 3, show no structural transition within the temperature range under study (300–850 °C). Good agreement factors were reached at the different temperatures for the mentioned simple-perovskite structural model. Fig. 3 illustrates the good agreement between the observed and calculated NPD patterns for $SrMo_{0.9}Co_{0.1}O_{3-\delta}$ at 300, 600 and 850 °C. Table 1 also summarizes the results obtained from the refinements at the different temperatures for $SrMo_{0.9}Co_{0.1}O_{3-\delta}$.

The thermal evolution of the oxygen content in vacuum was followed by NPD. Fig 4 illustrates the temperature dependence of the concentration of oxygen vacancies (δ) and unit-cell parameters for $SrMo_{0.9}Co_{0.1}O_{3-\delta}$. As expected, the unit-cell parameters increase with temperature from $a = 3.97029(6)$ Å at 25 °C to $a = 3.9927(11)$ Å at 850 °C (Fig. 4a). On the other hand, the oxygen content slightly

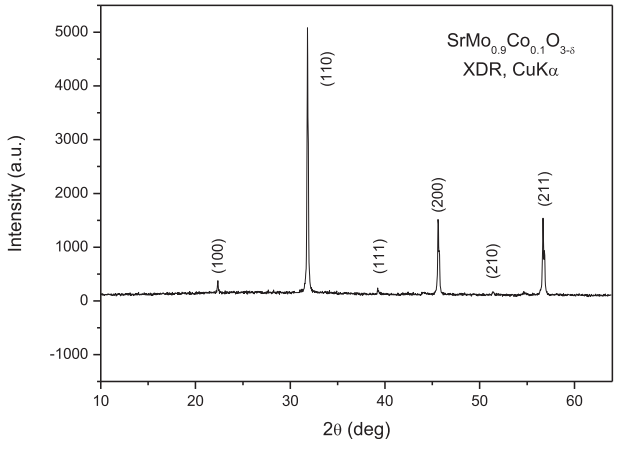

Fig. 1. XRD pattern with Cu K_α radiation for $SrMo_{0.9}Co_{0.1}O_{3-\delta}$, characteristic of a pure cubic perovskite phase.

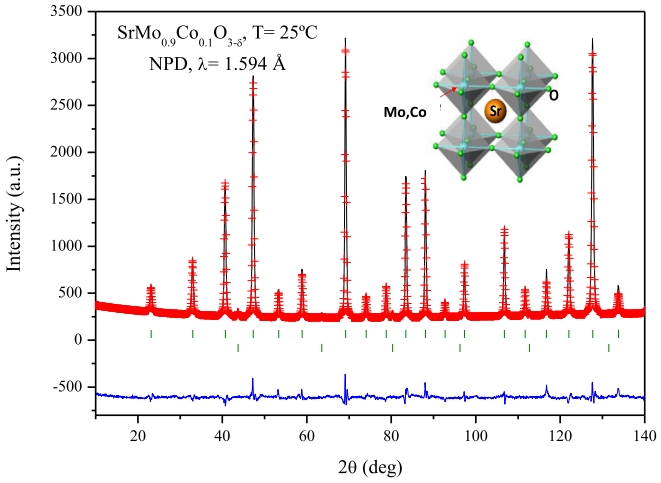

Fig. 2. Observed (crosses), calculated (full line) and difference (at the bottom) NPD profile for $SrMo_{0.9}Co_{0.1}O_{3-\delta}$ at 25 °C, refined in the cubic *Pm-3m* space group. The vertical markers correspond to the allowed Bragg reflections. The second series of Bragg reflections correspond to vanadium from the sample holder.

Table 1
Unit-cell, thermal parameters and selected distances (Å) for $SrMo_{0.9}Co_{0.1}O_{3-\delta}$ in cubic *Pm-3m* (no. 221) space group, from NPD data at 25, 300, 600 and 850 °C. Sr is placed at 1*b* (1/2, 1/2, 1/2), (Mo,Co) at 1*a* (0, 0, 0) and O1 at 3*d* (1/2, 0, 0) positions.

	25	300	600	850
$SrMo_{0.9}Co_{0.1}O_{3-\delta}$				
a (Å)	3.97029(6)	3.97369(4)	3.9821(10)	3.9927(11)
V (Å^3)	62. 584(2)	62.795(1)	63.145(3)	63.651(3)
Sr 1b (1/2,1/2,1/2)				
B_{iso}	0.725(3)	0.902(3)	1.748(6)	2.056(7)
f_{occ}	1.00	1.00	1.00	1.00
Mo/Co 1a (0,0,0)				
B_{iso}	0.131(3)	0.191(2)	0.437(5)	0.682(5)
Mo/Fe f_{occ}	0.92(1)/0.08(1)	0.92/0.08	0.92/0.08	0.92/0.08
O1 3d (1/2,0,0)				
B_{iso}	0.647(2)	0.787(1)	1.855(4)	2.212(4)
f_{occ}	1.00(1)	0.998(1)	0.993(1)	0.990(1)
Reliability factors				
χ^2	5.24	4.47	3.00	2.55
R_p (%)	4.08	3.38	2.60	2.47
R_{wp} (%)	5.24	4.28	3.33	3.12
R_{exp} (%)	2.25	2.03	2.43	2.44
R_I (%)	5.57	4.74	7.16	7.05
Distances (Å)				
(Sr) – (O1)	2.8070(3)	2.8096(2)	2.8188(5)	2.8273(6)
(Mo/Co) – (O1)	1.9856(3)	1.9881(2)	1.9941(5)	1.9984(6)

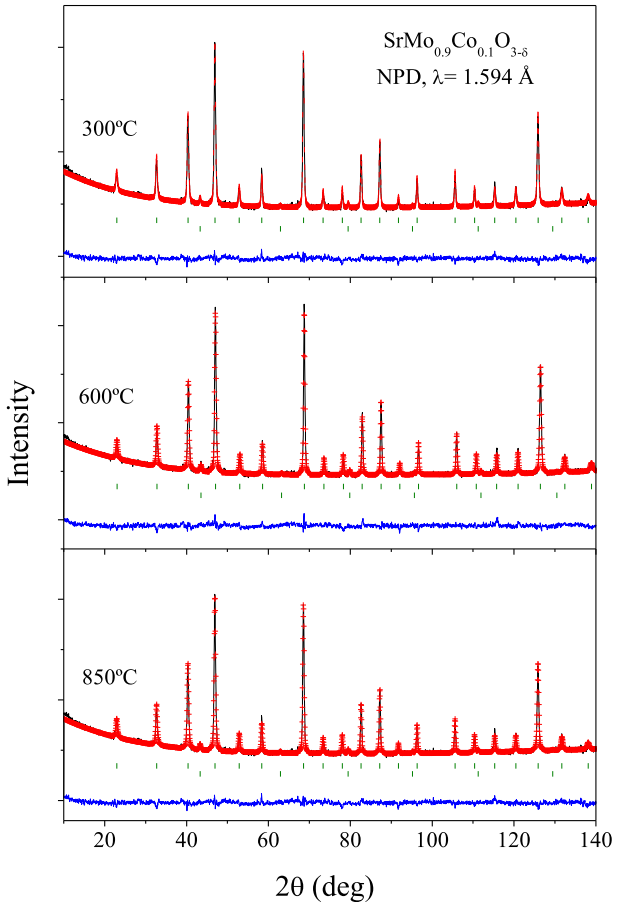

Fig. 3. Observed (crosses), calculated (full line) and difference (at the bottom) NPD profile for $SrMo_{0.9}Co_{0.1}O_{3-\delta}$ at 300, 600 and 850 °C in vacuum ($P_{O_2} = 10^{-6}$ Torr), refined in the cubic *Pm-3m* space group. The vertical markers correspond to the allowed Bragg reflections. The second series of Bragg reflections correspond to vanadium from the sample holder.

decreases when heating the sample in vacuum from $SrMo_{0.9}Co_{0.1}O_{3.00(1)}$ at room temperature to $SrMo_{0.9}Co_{0.1}O_{2.970(3)}$ at 850 °C (Fig. 4b). This fact suggests that the mixed-valence Mo(IV)–Mo(V) observed at room temperature becomes reduced to Mo(IV) upon heating, generating the wanted oxygen vacancies. These vacancies are essential to drive the required O^{2-} motion in a MIEC oxide. Besides, the isotropic displacement factors (B_{iso}) of the oxygen atoms increase from 0.647(2) Å^2 (25 °C) to 2.212(4) Å^2 (850 °C), as illustrated in Fig. 4b. This increment indicates a high mobility or chemical lability of these oxygen atoms, thus suggesting a high ionic conductivity at the working temperatures of the SOFC (700–850 °C).

3.2. Thermal analysis (TGA)

The thermal evolution of the sample was studied by recording the TGA curve. Heating $SrMo_{0.9}Co_{0.1}O_{3-\delta}$ in oxidizing (oxygen) atmosphere leads to the oxidation of this material to give $SrMo_{0.9}Co_{0.1}O_{4-\delta}$ with a scheelite-type crystal structure. Fig. 5 shows the thermal analysis curve obtained in O_2, displaying the incorporation, in an abrupt way, of 0.93 oxygen atoms in the 400–500 °C temperature range, which reveals an oxygen-defective scheelite phase with formula $SrMo_{0.9}Co_{0.1}O_{3.93}$. The inset of Fig. 5 illustrates the crystal structure of the scheelite oxide. A thermal treatment of the resulting scheelite phase in reducing (H_2(5%)/N_2) atmosphere restores the perovskite phase, thus confirming the required reversibility upon cycling in oxidizing–reducing atmospheres.

In order to carry out a more detailed investigation of the structural details of the new oxygen-defective scheelite, a neutron powder diffraction (NPD) study at room temperature was performed. The crystal structure was defined in the $I4_1/a$ space group (No. 88), $Z = 4$; in this context, Sr atoms are located at 4*b* (0,1/4,5/8), Mo and Co are distributed at random at 4*a* (0,1/4,1/8) and oxygen atoms O1 are located at 16*f* (*x*,*y*,*z*) sites. The occupancy factors of the oxygen atoms were refined in the final run; the introduction at the B sublattice of Co ions with a smaller oxidation state than Mo ions, is effective in the creation of oxygen vacancies, yielding a new oxygen-deficient scheelite. The refinement of the occupancy factors of oxygen (O) and Mo/Co atoms leads to the final $SrMo_{0.93(1)}Co_{0.07(1)}O_{3.896(1)}$ stoichiometry, which is in good agreement to the value obtained from the TGA ($SrMo_{0.9}Co_{0.1}O_{3.93}$). Fig. 6 illustrates the good agreement between the observed and calculated NPD patterns for $SrMo_{0.93(1)}Co_{0.07(1)}O_{3.896(1)}$ at room temperature. Table 2 summarizes the unit-cell, atomic, thermal parameters, discrepancy factors, interatomic distances and angles after the Rietveld refinements of the scheelite phase at room temperature.

Assuming hexavalent Mo for the oxidized scheelite phase, Co exhibits a valence of +3.03 for the formula $SrMo_{0.93(1)}Co_{0.07(1)}O_{3.896(1)}$ determined from NPD data. The unit-cell volume for the sample at room temperature is 347.00(14) Å^3, which is much smaller than the value reported in the literature for $SrMoO_4$ scheelite, $V = 349.19$ Å [25]; the presence of a substantial amount of oxygen vacancies is related to the observed shrinkage of the unit

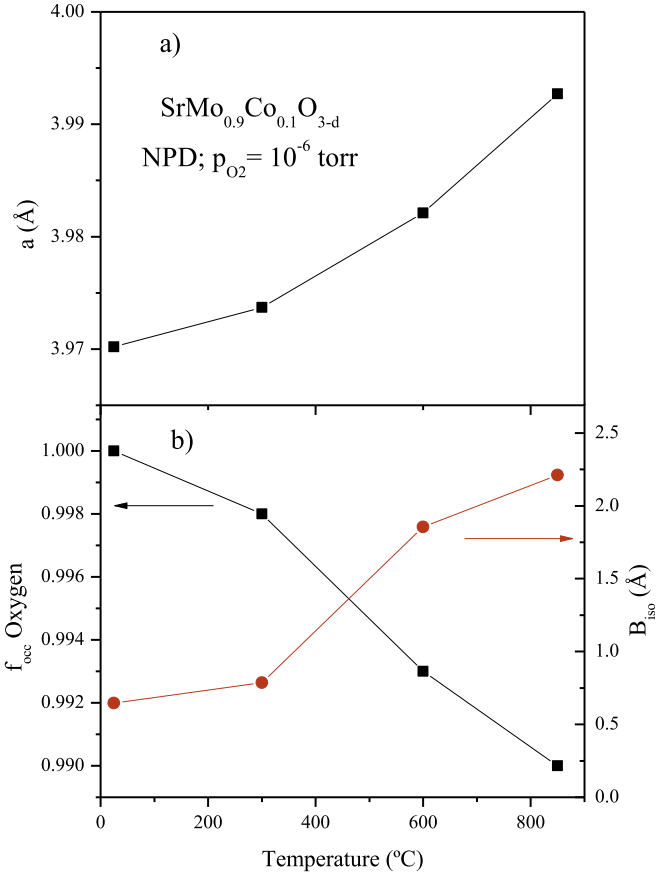

Fig. 4. Thermal variation of a) unit-cell parameter and b) oxygen occupancy factor (left axis) and isotropic displacement factor for O atoms (right axis), from *in-situ* NPD data.

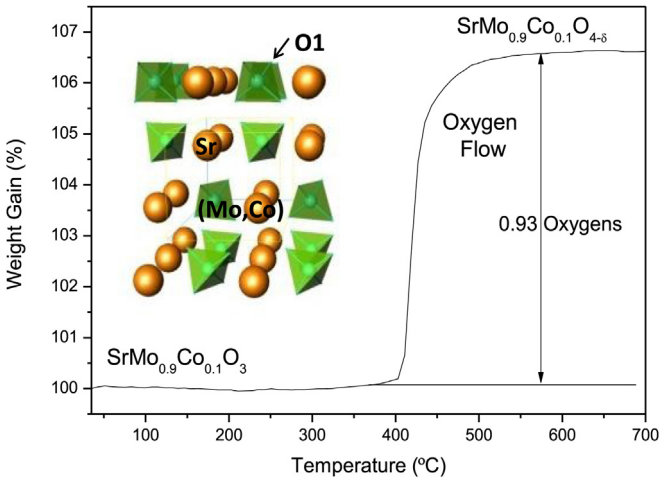

Fig. 5. Thermal analysis in O_2 flow (TG curve) of the $SrMo_{0.9}Co_{0.1}O_{3-\delta}$ perovskite, showing an oxidation step to a deficient-scheelite phase. The inset illustrates the scheelite crystal structure.

cell. The <Mo,Cr–O> bond lengths are slightly smaller (1.76418(2) Å) with respect to those given for the parent $SrMoO_4$ scheelite [25], of 1.767 Å, which is a result of the chemical pressure due to the collapse of the unit cell upon the introduction of oxygen vacancies in the lattice, resulting in a stretching of the tetrahedral Mo/Co group.

3.3. Thermal expansion

Aiming to determine the mechanical compatibility of our material with the other cell components, the measurement of the thermal expansion of a dense ceramic was carried out in a 5%H_2 atmosphere. The thermal expansion of the perovskite phase was measured in sintered pellets, first preheated in air at 900 °C for 12 h and finally reduced in a 5%H_2 flow at 1000 °C for 15 h. A dilatometric analysis was performed between 35 and 850 °C for several cycles; the data were only recorded during the heating runs. Fig. 7 shows no abrupt changes in the thermal expansion of nominal $SrMo_{0.9}Co_{0.1}O_{3-\delta}$ perovskite in all the temperature range under

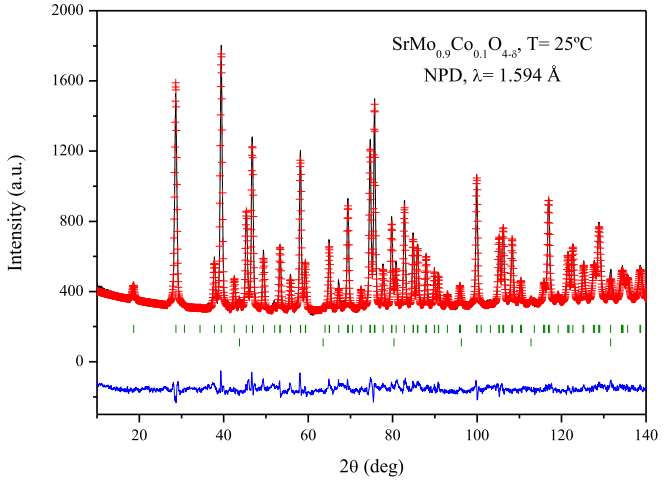

Fig. 6. Observed (crosses), calculated (full line) and difference (at the bottom) NPD profile for nominal $SrMo_{0.9}Co_{0.1}O_{4-\delta}$ scheelite phase, refined in the tetragonal $I4_1/a$ space group. The vertical markers correspond to the allowed Bragg reflections. The second series of Bragg reflections correspond to vanadium from the sample holder.

Table 2
Unit-cell, thermal parameters, interatomic distances and angles for $SrMo_{0.9}Co_{0.1}O_{4-\delta}$ scheelite structure in the tetragonal $I4_1/a$ (No. 88) space group from NPD data at 25 °C. Sr is placed at 4*b* (0,1/4,5/8); Mo/Co at 4*a* (0,1/4,1/8), O at 16*f* (*x*,*y*,*z*) sites.

	$SrMo_{0.9}Co_{0.1}O_{4-\delta}$
a (Å)	5.3764(1)
b (Å)	=
c (Å)	12.0046(4)
V (Å^3)	347.00(14)
Sr 4b (0,1/4,5/8)	
B_{iso} (Å^2)	0.529(5)
f_{occ}	1.00
Mo/Co 4a (0,1/4,1/8)	
B_{iso} (Å^2)	0.431(5)
Mo/M f_{occ}	0.93(1)/0.07(1)
O1 16f (*x*,*y*,*z*)	
x	0.23648(2)
y	0.11521(2)
z	0.04293(1)
B_{iso} (Å^2)	0.663(2)
f_{occ}	0.974(0)
Reliability factors	
χ^2	3.92
R_p (%)	3.13
R_{wp} (%)	3.89
R_{exp} (%)	1.99
R_{Bragg} (%)	6.91
Distances (Å)	
Sr–O (×4)	2.61406(3)
(×4)	2.56837(4)
<Sr–O>	2.5912
(Mo,Co) (×4)	1.76418(2)
Angles (°)	
O–Mo,Co–O	108.173(2)
O–Mo,Co–O	112.101(2)

measurement. The thermal expansion coefficient (TEC) measured under 5%H_2/95%N_2 atmosphere between 300 and 850 °C is 12.8×10^{-6} K^{-1}; this value is in good agreement with that obtained from neutron diffraction data in the heating run, 13.8×10^{-6} K^{-1} (between 300 and 850 °C). In addition, this value perfectly matches with the values usually displayed by SOFC electrolytes (LSGM, TEC = 12.5×10^{-6} K^{-1}) [26].

Also, the thermal expansion of the oxygen-defective $SrMo_{0.9}Co_{0.1}O_{4-\delta}$ scheelite phase was measured in sintered pellets, preheated in air at 900 °C for 12 h, as illustrated in Fig. 7. The

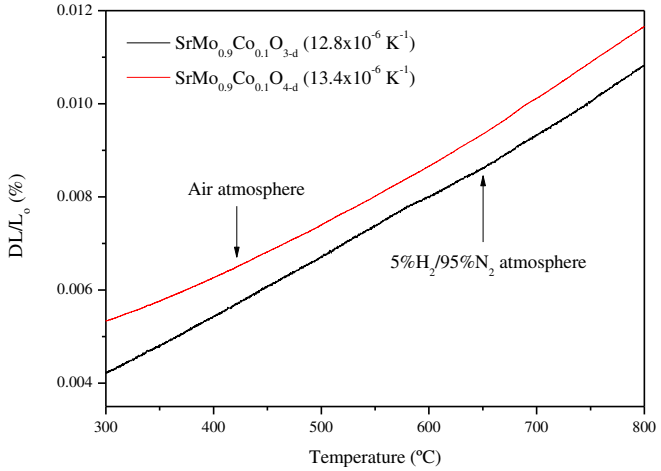

Fig. 7. Thermal expansion determined by dilatometry of the $SrMo_{0.9}Co_{0.1}O_{3-\delta}$ and $SrMo_{0.9}Co_{0.1}O_{4-\delta}$ phases.

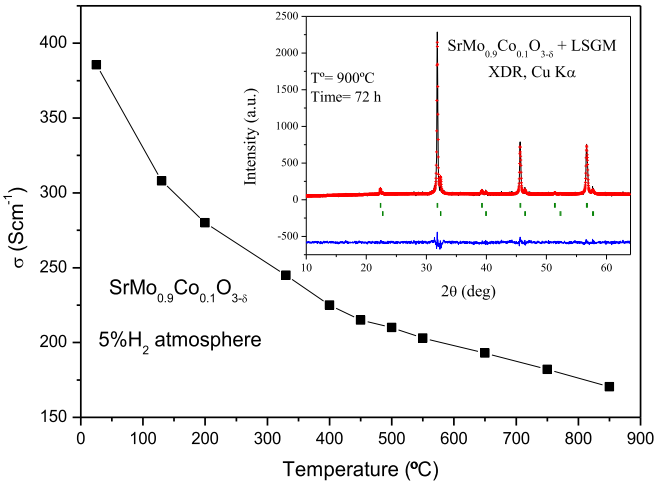

Fig. 8. *dc*-Conductivity as a function of temperature for $SrMo_{0.9}Co_{0.1}O_{3-\delta}$. The inset shows the Rietveld-refined XRD profiles of a mixture of $SrMo_{0.9}Co_{0.1}O_{3-\delta}$ and LSGM after a thermal treatment at 900 °C for 72 h in H_2(5%)/N_2(95%), showing no reaction products between both phases. The first and second series of Bragg positions correspond to $SrMo_{0.9}Co_{0.1}O_{3-\delta}$ and LSGM, respectively.

determined TEC is 13.4 × 10^{-6} K^{-1} when heating the sample between 300 and 850 °C in air, very similar to that obtained for the reduced perovskite (12.8 × 10^{-6} C^{-1}). The similar values for the oxidized and reduced phases are crucial to avoid cracking problems during the heating ramp and the SOFC operation. The material was fired on the LSGM pellet in the oxidized phase and then transformed to the reduced phase as the temperature increased under 5%H_2 atmosphere.

3.4. Electrical conductivity and chemical compatibility

Fig. 8 shows the thermal variation of the electrical conductivity of the $SrMo_{0.9}Co_{0.1}O_{3-\delta}$ perovskite measured in sintered bars (10 mm large × 3 mm width × 3 mm high) in 5% H_2/95% N_2 atmosphere by the *dc* four-probe method; the bars were sintered during 12 h at 1000 °C in 5% H_2/95%N_2 atmosphere. The perovskite material shows a metallic-like conductivity under reducing conditions in all the temperature range (25–850 °C); the conductivity

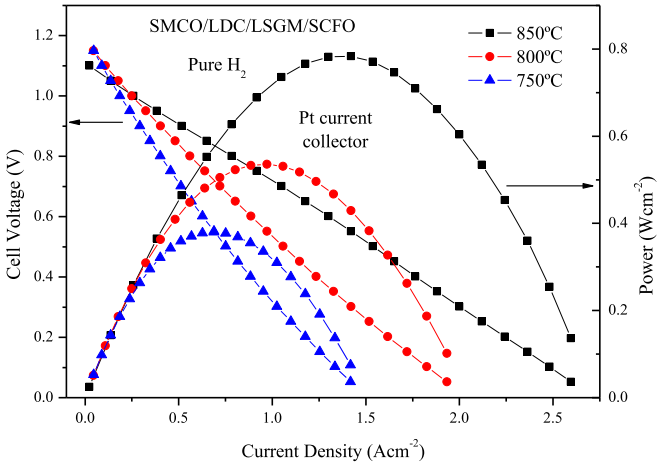

Fig. 9. Cell voltage (left axis) and power density (right axis) as a function of the current density for the test cell with the configuration SMCO/LDC/LSGM/SCFO in pure H_2 measured at T = 750, 800 and 850 °C with Pt as current collector.

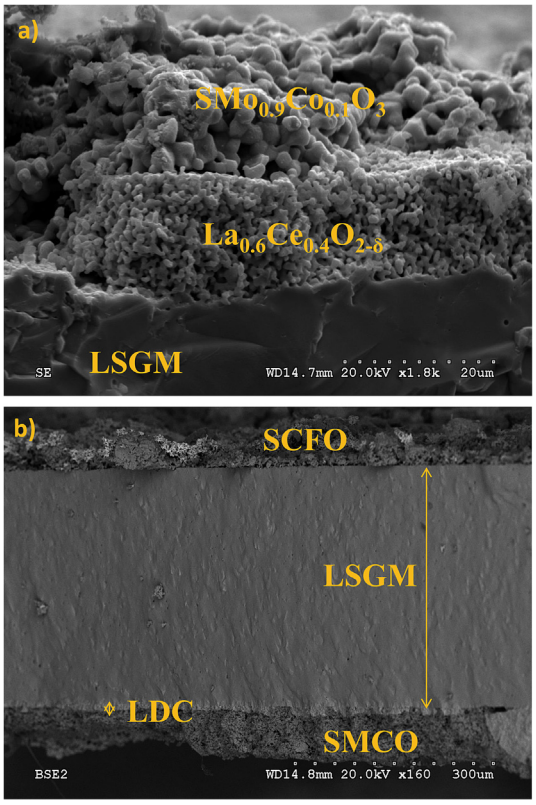

Fig. 10. Backscattered SEM images of a) interface SMCO/LDC/LSGM and b) interface SMCO/LSGM/SCFO after the single cell test.

at 50 °C reaches a maximum value of 386 S cm^{-1}, while at 850 °C it decreases to 170 S cm^{-1}. At the SOFC working temperature, between 700 and 850 °C, the conductivity spans from 190 to 170 S cm^{-1}, overcoming the requirement (150 S cm^{-1}) for a good anode material. As expected, when the perovskite phase is oxidized to the scheelite structure it becomes an insulator.

The chemical compatibility of $SrMo_{0.9}Co_{0.1}O_{3-\delta}$ with the LSGM electrolyte was also checked by firing mixtures of both powdered materials at 900 °C in H_2(5%)/N_2(95%) atmosphere for 72 h. The inset of Fig. 8 shows a Rietveld analysis by XDR of the product, consisting of a mixture of both unaltered perovskite phases, which is essential for the good performance of the anode material during the cell operation.

3.5. Fuel-cell tests

The performance of the $SrMo_{0.9}Co_{0.1}O_{3-\delta}$ oxide as anode in SOFC was tested in single cells in an electrolyte-supported configuration using a 300-μm-thick LSGM electrolyte. Fig. 9 illustrates the cell voltage and power density as a function of current density at 750, 800 and 850 °C for the single cells fed with pure H_2. The maximum power densities generated by the cell are 380, 545 and 793 mW cm^{-2}, respectively. This excellent performance is due to the good compromise between determining factors. The catalytic activity is driven by the presence of molybdenum, which is apparently responsible for the catalytic oxidation of the fuel, as it has been observed in other Mo-containing anodes [9]. The presence of oxygen vacancies together with a good electronic conductivity demonstrates that this oxide plays an excellent role as a MIEC electrode.

3.6. Scanning electron microscopy

Fig. 10a shows the cross-section micrograph of the anode–buffer-layer–electrolyte interface after the single-cell tests analyzed by scanning electron microscopy (SEM). It is estimated that the thicknesses of the SMCO and LDC layers are approximately 10 μm and the average grain sizes of the particles are about 1 μm. In addition, the SMCO exhibits a good porosity, which is one of the essential requirements for optimal anode materials as it favors the diffusion and oxidation process of the fuel throughout the bulk of the anode.

Fig. 10b illustrates the cross-section micrograph of the anode–electrolyte–cathode interface after the single-cell tests. The SEM image shows a uniform and dense electrolyte layer, without cracks or fractures; the thickness of the LSGM is approximately 300 μm. As well, no formation of fractures or delaminations in both electrodes is observed after the single-cell test. The brightest parts in Fig. 10b correspond to the platinum (Pt) used to deposit the gauze at the anodic and cathodic sizes.

4. Conclusion

$SrMo_{0.9}Co_{0.1}O_{3-\delta}$ oxide can be successfully utilized as anode material in single SOFC cells in an electrolyte (LSGM)-supported configuration; a maximum power density close 800 mW cm^{-2} was obtained at 850 °C with pure H_2 as fuel, using platinum as current collector (gauze and paste). The crystal structure has been refined at room temperature in the cubic *Pm-3m* space group from NPD data, and no structural transitions has been observed in the investigated temperature interval (25–850 °C). The sufficiently high number of oxygen vacancies along with high isotropic displacement factors suggests a high ionic conductivity at the working temperatures.

The excellent performance relies on the high electronic conductivity derived from the parent $SrMoO_3$ and the oxygen vacancies induced upon Co doping, providing the suitable ionic transport; the result is an excellent catalyst for hydrogen oxidation. The electrical characterization evidences a metallic behavior with high conductivity values, more than 150 S cm^{-1} at the working temperatures (700–850 °C). The thermal expansion coefficients for the perovskite and scheelite phases, of 12.8 × 10^{-6} and 13.4 × 10^{-6} K^{-1}, respectively, are very close to those of the usual SOFC electrolytes at the working temperatures. The thermal analysis along with room temperature NPD data allowed identifying a new deficient-scheelite phase with formula $SrMo_{0.93(1)}Co_{0.07(1)}O_{3.896(1)}$. This new phase exhibits a total reversibility with the perovskite phase upon oxidation–reduction processes; this fact is requested for the cyclability of the cells thus avoiding cracking problems during the cell operation.

Acknowledgments

The authors thanks the Robert A. Welch Foundation of Houston, TX and the Spanish “ Ministerio de Ciencia e Innovación” (MICINN-Project MAT2010-16404) for the financial support. We are grateful to ILL (Institut Laue-Langevin, Grenoble) for making the beamtime available.

References

[1] J.P.P. Huijsmans, F.P.F. Van Berkel, G.M. Christie, J. Power Sources 71 (1998) 107.
[2] D. Brett, A. Atkinson, N.P. Brandon, S.J. Skinner, Chem. Soc. Rev. 37 (2008) 1568.
[3] S.P. Jiang, S.H. Chan, Mater. Sci. Technol. 20 (2004) 1109.
[4] B.C.H. Steele, I. Kelly, M. Middleton, R. Rudkin, Solid State Ionics 28–30 (1988) 1547.
[5] Y. Matsuzaki, I. Yasuta, Solid State Ionics 132 (2000) 261.
[6] Chunwen Sun, Ulrich Stimming, J. Power Sources 171 (2007) 247–260.
[7] H. Yokokawa, N. Sakai, T. Horita, K. Yamaji, Fuel Cells 1 (2001) 117–131.
[8] J.B. Goodenough, J. Appl. Phys. 37 (1966) 1415–1422.
[9] S.-E. Hou, J.A. Alonso, J.B. Goodenough, J. Power Sources 195 (1) (2010) 280–284.
[10] A. Aguadero, J.A. Alonso, D. Perez-Coll, C. de la Calle, M.T. Fernandez-Diaz, J.B. Goodenough, Chem. Mater 22 (2010) 789–798.
[11] S.-E. Hou, J.A. Alonso, S. Rajasekhara, M.J. Martinez-Lope, M.T. Fernandez-Diaz, J.B. Goodenough, Chem. Mater 22 (2010) 1071.
[12] S. Hayashi, R. Aoki, Mater Res. Bull. 13 (3) (1979) 409.
[13] J. Kubo, W. Ueda, Mater Res. Bull. 44 (4) (2009) 906.
[14] B.L. Chamberland, P.S. Danielson, J. Solid State Chem. 3 (1971) 243.
[15] R. Martínez-Coronado, J.A. Alonso, A. Aguadero, M.T. Fernandez-Diaz, J. Power Sources 208 (2012) 153–158.
[16] R. Martinez-Coronado, J.A. Alonso, A. Aguadero, M.T. Fernandez-Diaz, Int. J. Hydrogen Energy 39 (8) (2014) 4067–4073.
[17] V. Dusastre, J.A. Kilner, Solid State Ionics 126 (1999) 163–174.
[18] M.J. Jorgensen, S. Primdahl, M. Mogensen, Electrochim. Acta 44 (1999) 4195–4201.
[19] J.A. Alonso, M.J. Martínez-Lope, A. Aguadero, L. Daza, Prog. Solid State Chem. 36 (2008) 134–150.
[20] H.M. Rietveld, J. Appl. Crystallogr. 2 (1969) 65–71.
[21] J. Rodríguez-Carvajal, Physica B 192 (1993) 55–69.
[22] R.B. Macquart, B.J. Kennedy, M. Avdeev, J. Solid State Chem. 183 (2010) 250–255.
[23] R.D. Shannon, Acta Crystallogr. A32 (1976) 751–767.
[24] A. Aguadero, J.A. Alonso, R. Martinez-Coronado, M.J. Martinez-Lope, M.T. Fernandez-Diaz, J. Appl. Phys. 109 (2011) 034907-1–034907-6.
[25] E. Gürmen, E. Daniels, J.S. King, J. Chem. Phys. 55 (1971) 1093.
[26] M. Feng, J.B. Goodenough, Eur. J. Solid State Inorg. Chem. 31 (1994) 663.